Rapid viscoelastic changes are a hallmark of early leukocyte activation

Alexandra Zak, Sara Violeta Merino-Cortés, Anaïs Sadoun, Farah Mustapha, Avin Babataheri, Stéphanie Dogniaux, Sophie Dupre-Crochet, Elodie Hudik, Hai-Tao He, Abdul Barakat, et al.

Rapid viscoelastic changes are a hallmark of early leukocyte activation.

Alexandra Zak[1,2], Sara Violeta Merino-Cortés[3], Anaïs Sadoun[4,5,6], Farah Mustapha[4,5,6,7], Avin Babataheri[1], Stéphanie Dogniaux[8], Sophie Dupré-Crochet[2], Elodie Hudik[2], Hai-Tao He[9], Abdul I Barakat[1], Yolanda R Carrasco[3], Yannick Hamon[9], Pierre-Henri Puech[4,5,6], Claire Hivroz[8], Oliver Nüsse[2], and Julien Husson[1]*.

1 LadHyX, CNRS, Ecole polytechnique, Institut Polytechnique de Paris, 91120, Palaiseau, France.
2 Institut de Chimie Physique, CNRS UMR8000, Université Paris-Saclay, 91405, Orsay, France.
3 B cell Dynamics Laboratory, Department on Immunology and Oncology, Centro Nacional de Biotecnología (CNB)-CSIC, Madrid, Spain.
4 Aix Marseille University, LAI UM 61, Marseille, F-13288, France.
5 Inserm, UMR_S 1067, Marseille, F-13288, France.
6 CNRS, UMR 7333, Marseille, F-13288, France.
7 Centre Interdisciplinaire de Nanoscience de Marseille (CINaM), CNRS, Aix Marseille University, Marseille, F-13009 France.
8 Institut Curie, PSL Research University, INSERM U932, Integrative analysis of T cell activation team, 26 rue d'Ulm, 75248, Paris Cedex 05, France.
9 Aix Marseille University, CNRS, INSERM, CIML, Marseille, France.
* corresponding author, julien.husson@ladhyx.polytechnique.fr, https://cellmechanics.jimdofree.com/

Abstract

To accomplish their critical task of removing infected cells and fighting pathogens, leukocytes activate by forming specialized interfaces with other cells. The physics of this key immunological process are poorly understood, but it is important to understand them as leukocytes have been shown to react to their mechanical environment. Using an innovative micropipette rheometer, we show in three different types of leukocytes that, when stimulated by microbeads mimicking target cells, leukocytes become up to ten times stiffer and more viscous. These mechanical changes start within seconds after contact and evolve rapidly over minutes. Remarkably, leukocyte elastic and viscous properties evolve in parallel, preserving a well-defined ratio that constitutes a mechanical signature specific to each cell type. Our results indicate that simultaneously tracking both elastic and viscous properties during an active cell process provides a new way to investigate cell mechanical processes. Our findings also suggest that dynamic immuno-mechanical measurements can help discriminate between leukocyte subtypes during activation.

Significance

The mammalian immune response is largely based on direct interactions between white blood cells (leukocytes) and pathogens, inert particles or other host cells. Mechanical properties of leukocytes regulate their migration in the microcirculation to reach their targets, and their interaction with these targets. Yet, these mechanical properties and their evolution upon leukocyte activation remain poorly studied. We developed a micropipette-based rheometer to track cell viscous and elastic properties. We show that leukocytes become up to ten times stiffer and more viscous during their activation. Elastic and viscous properties evolve in parallel, preserving a ratio characteristic of the leukocyte subtype. These mechanical measurements set up a complete picture of the mechanics of leukocyte activation and provide a signature of cell function.

Introduction

The understanding of cell mechanics has progressed with the development of micromanipulation techniques such as micropipette aspiration (1), indentation techniques (2), and others (3). Microfluidics-based approaches such as real-time deformability cytometry now allow high-throughput mechanical measurements (4, 5). Yet, these techniques make it difficult to track mechanical changes in cells stimulated by soluble molecules (6, 7), and even more difficult when cells are stimulated by activating surfaces or partner cells (8).

Tracking these changes can bring a wealth of information on cell function in healthy conditions and diseases. Here we illustrate this by focusing on white blood cells (leukocytes). These cells, among other functions, fight infected cells or pathogens, remove dead cells, or identify antigens at the surface of other cells and eventually build an immune response against a detected threat. To do so, leukocytes activate by forming with other cells specialized interfaces called immunological synapses. Different leukocytes form different types of synapses, which share several molecular (9) but also mechanical features. One of these mechanical features is force generation, which is now well documented in different types of leukocytes. For instance, we have shown that a T lymphocyte generates forces when forming a synapse (10, 11). Others recently showed that B cells generate traction forces during activation (12, 13), and Evans et *al.* quantified decades ago contractile forces generated during phagocytosis (14). The role of these forces is still an open question. Their suggested functions, such as allowing a tight cell-cell contact or probing the mechanical properties of the opposing surface, place these forces at the core of leukocyte activation (15, 16). In this study, we focus on another mechanical feature: changes in leukocyte viscoelasticity during their activation. These changes have been shown to exist in T cells, phagocytes, and B cells. We have shown that during activation, T cells stiffen (17). Pioneering observations showed that during phagocytosis, the cortical tension of a phagocyte increases dramatically while this cell engulfs its prey (14, 18), and more recent observations confirmed mechanical stiffening of leukocytes during phagocytosis (19). We also recently quantified elastic changes in B cells during activation (20).

As for force generation, the function of the mechanical properties of leukocytes during activation is not yet understood and open to speculation (see Discussion). Yet, it is important to quantify and describe them for two reasons. First, we need a complete picture of the mechanics of leukocyte activation to properly incorporate mechanics into currently proposed models of the activation of the different types of leukocytes. Second, beside the fundamental interest of understanding these mechanical changes, they can have very important consequences in the context of disease. Indeed, mechanical properties of leukocyte dictate how easily leukocytes migrate in or out of tissue or flow in small blood vessels (21), so changes of these properties can perturb physiological processes. For instance, circulating neutrophils stimulated by proinflammatory molecules exhibit changes in their mechanical properties (22, 23), which contributes to their trapping in pulmonary vasculature in lung diseases such as acute respiratory distress syndrome (23, 24). Being trapped or slowed down while traveling in a capillary can be due to an increased cell stiffness, but also to an increased cell viscosity. Understanding cell viscous properties is thus also important, although viscous properties are much less explored than elastic ones due to inherent difficulties in quantifying them.

Most measurements of leukocyte mechanics, including the ones mentioned above, were focused on elastic and not viscous properties. However, it was recognized decades ago that leukocytes are viscoelastic and not only elastic (25–27), so in many situations we miss an important aspect of leukocyte mechanics. Fabry *et al.* (28) and others have shown that one can expect the viscous properties of leukocytes to be linked to their elastic properties. It was recognized that resting leukocytes such as neutrophils (27, 29) and macrophages (30) conserve a ratio of cortical tension to cell viscosity of about 0.2-0.3 μm/s, even though macrophages can be ten times more tensed than neutrophils. The ratio of viscous to elastic properties seems to be constrained within a rather narrow range of values, and many studies showed this peculiar aspect of biological matter in various cell types (28, 31, 32). Here, we asked if for a given cell type, elastic and viscous properties of leukocytes respected a relationship while they were both evolving over time. To do so, we quantified the evolution of both elastic

and viscous properties during the activation of three types of leukocytes. We used a micropipette rheometer to activate leukocytes with standardized activating antibody-covered microbeads (17, 33–35), and we further probed early mechanical changes occurring in leukocyte-target cell contacts by using Atomic Force Microscopy in Single Cell Force Spectroscopy mode (36).

Materials and Methods

Micropipette rheometer

The rheometer was build based on the evolution of our profile microindentation setup(37) and Micropipette Force Probe(17, 33, 38). Micropipettes were prepared as described previously(17, 33, 37, 38) by pulling borosilicate glass capillaries (Harvard Apparatus, Holliston, MA, USA) with a P-97 micropipette puller (Sutter Instruments, Novato, CA, USA), cutting them with an MF-200 microforge (World Precision Instruments, Sarasota, FL, USA) and bending them at a 45° angle with an MF-900 microforge (Narishige, Tokyo, Japan). Micropipettes were held by micropipette holders (IM-H1, Narishige) placed at a 45° angle relative to a horizontal plane, so that their tips were in the focal plane of an inverted microscope under brightfield or DIC illumination (T cells: TiE ; PLB cells: Ti2, Nikon Instruments, Tokyo, Japan) equipped with a 100× oil immersion, 1.3 NA objective (Nikon Instruments) and placed on an air suspension table (Newport). The flexible micropipette was linked to a non-motorized micropositioner (Thorlabs, Newton, NJ, USA) placed on top of a single-axis stage controlled with a closed loop piezo actuator (TPZ001; Thorlabs). The bending stiffness k of the flexible micropipette (about 0.2 nN/µm) was measured against a standard microindenter previously calibrated with a commercial force probe (model 406A; Aurora Scientific, Aurora, ON, Canada). Once the activating microbead was aspirated by the flexible micropipette, the cell held by the stiff micropipette was brought in adequate position using a motorized micromanipulator (MP-285; Sutter Instruments). Experiments were performed in glass-bottom Petri dishes (Fluorodish, WPI, Sarasota, FL, USA). Images were acquired using a Flash 4.0 CMOS camera (for T cells), or a SPARK camera (PLB cells), both from Hamamatsu Photonics, Hamamatsu City, Japan. In order to perform rheological experiments, the setup automatically detects the position of the bead at the tip of the force probe at a rate of 400-500 Hz and imposes the position of the base of the flexible micropipette by controlling the position of the piezo stage. The deflection of the force probe is the difference between the position of the bead and the position of the piezo stage. Thus, the force applied to the cell is the product of this deflection by the bending stiffness k. A retroaction implemented in Matlab (Mathworks) controlling both the camera via the Micromanager software (39) and the piezo stage moves the latter in reaction to the measurement of the bead position in order to keep a desired deflection of the cantilever: a controlled force is applied to the cell at any given time. Experiments were performed at room temperature to avoid thermal drift. Qualitative behavior of T cell and PLB cells is unchanged at 37°C (not shown). We quantified the fluid drag due to micropipette translation (Suppl. Mat. 1) and the potential effect of fast cell deformation on our rheological measurements (Suppl. Mat. 2). The accuracy when measuring the phase shift depends on the acquisition frequency of both force and cell deformation (x_{tip}), which is 400-500 Hz depending on the size of the region of interest chosen for the acquisition. This leads to a time resolution of 2-2.5 ms. The measured loss tangent had a typical value of $\eta = \frac{K''}{K'} = tan(\varphi) \approx 0.3 - 0.5$, i.e. $\varphi \approx 0.3 - 0.5$. When expressed in seconds instead of radians, this phase lag represents a delay $\Delta t = \frac{\varphi}{2\pi} T$, where $T = 1s$ is the period of the oscillatory force modulation, which leads to $\Delta t = 46 - 74\ ms$. This is reasonably long when compared to our time resolution so as to be accurately measured. Note that the uncertainty on the phase lag influenced more K'' than K', because K'' is proportional to $sin(\varphi)$ while K' is proportional to $cos(\varphi)$. *Data analysis.* Rheological measurements were analyzed by post-processing using a custom-made Python code. During force modulation sinusoidal x_{tip} signal was fitted every 0.5-1 period interval over a window that was 1.5-2.5 periods long (i.e. every 0.5-1 second with a window of 1.5-2.5 seconds for a frequency of force modulation f=1 Hz) using a function corresponding to a linear trend with an added sinusoidal signal (two free parameters for the linear trend, two for the sinusoidal signal

when imposing the frequency f=1 Hz). Best fit was determined using classical squared error minimization algorithm in Python.

T cell experiments

Cells and reagents. Mononuclear cells were isolated from peripheral blood of healthy donors on a Ficoll density gradient. Buffy coats from healthy donors (both male and female donors) were obtained from Etablissement Français du Sang (EFS, Paris, France) in accordance with INSERM ethical guidelines. Human total CD4+ isolation kit (Miltenyi Biotech, 130-096-533) was used for the purification of T cells. Isolated T-cells were suspended in FBS: DMSO (90%:10% vol/vol) and kept frozen in liquid nitrogen. One to seven days before the experiment the cells were thawed. Experiments were performed in RPMI 1640 1x with GlutaMax, supplemented with 10% heat-inactivated fetal bovine serum (FBS) and 1% penicillin-streptomycin (all from Life Technologies ThermoFisher Scientifc, Waltham, MA), and filtered with (0.22 μm diameter-pores, Merck Millipore).

Beads. Dynabeads® Human T-Activator CD3/CD28 for T Cell Expansion and Activation from Gibco, were purchased from Thermo Fisher Scientific (ref. 11131D, Carlsbad, CA). These 4.5-μm, superparamagnetic polymer beads, coated with an optimized mixture of mouse anti-human monoclonal IgG antibodies against the CD3 and CD28 cell surface molecules of human T cells, mimic stimulation by an antigen presenting cell (APC). The CD3 antibody is specific for the epsilon chain of human CD3. The CD28 antibody is specific for the human CD28 co-stimulatory molecule, which is the receptor for CD80 (B7-1) and CD86 (B7-2). These beads induce the phosphorylation of several signaling proteins (17, 40). Control beads were non-coated 4.5-μm polystyrene beads.

B cell experiments

B cells. Primary B lymphocytes were isolated from spleens of adult C57BL/6J mice (10- to 20-week-old), purified by negative selection using the MACS kit (130-090-862) in the total splenocytes. Animal procedures were approved by the CNB-CSIC Bioethics Committee and conform to institutional, national and EU regulations. Cells were cultured in complete RPMI 1640-GlutaMax-I supplemented with 10% FCS, 1% penicillin-streptomycin, 0.1% β-mercaptoethanol and 2% sodium pyruvate (denominated hereafter as complete RPMI).

Beads. Silica beads (5 x 10^6; 5 μm diameter; Bangs Laboratories) were washed in distilled water (5,000 rpm, 1 min, RT), and incubated with 20 μl 1,2-dioleoyl-PC (DOPC) liposomes containing GPI-linked mouse ICAM-1 (200 molecules/μm^2) and biotinylated lipids (1000 molecules/μm^2) (10 min, RT), and washed twice with beads-buffer (PBS supplemented with 0.5% FCS, 2 mM $MgCl_2$, 0.5 mM $CaCl_2$, and 0.5 g/L D-Glucose). Then, lipid-coated beads were incubated with AF647-streptavidin (Molecular Probes) (20 min, RT) followed by biotinylated rat anti-κ light chain antibody (clone 187.1, BD Biosciences) (20 min, RT), used as surrogate antigen (su-Ag) to stimulate the B cell receptor. Control beads were coated with ICAM-1-containing lipids only (no su-Ag was added). The number of molecules/μm^2 of ICAM-1 and su-Ag/biotin-lipids was estimated by immunofluorometric assay using anti-ICAM-1 or anti-rat-IgG antibodies, respectively; the standard values were obtained from microbeads with different calibrated IgG-binding capacities (Bang Laboratories). The lipid-coated silica beads were finally re-suspended in complete RPMI before use. Such a use of lipid-coated silica beads as pseudo-APCs to study immune synapse formation, cell activation, proliferation and antigen extraction by B cells has been previously set up and reported by us (20, 41). They provide the adhesion ligand ICAM-1 for the integrin LFA-1, expressed at the B cell surface, and tethered BCR-stimulatory signal (su-Ag) in a fluid phospholipid environment.

PLB cell experiments

Cells and reagents. The human acute myeloid leukemia cell line PLB-985 is a subline of HL-60 cells based on STR fingerprinting (42, 43). Gene expression in the two lines is similar but not identical (44). PLB-985 cells were cultured in RPMI 1640 1X GlutaMax (Gibco) supplemented with 10% sterile heat-inactivated FBS and 1% sterile penicillin/streptomycin. Cells were passaged twice a week and differentiated into a neutrophil-like phenotype by adding 1.25 % (v/v) of dimethyl sulfoxide (DMSO, Sigma-

Aldrich) to the cell suspension the first day after passage and, in a second time, three days after while changing the culture media (45). Twenty four hours before experiments, 2000 U/ml IFN-γ (Immuno Tools) were added into the cell culture flask, cells were centrifuged for 3 min at 300g and resuspended in 0.22-µm filtered HEPES medium (140 mM NaCl, 5 mM KCl, 1 mM MgCl2, 2 mM CaCl2, 10 mM HEPES pH 7.4, 1.8 mg/mL glucose, and 1% heat-inactivated FBS ; filters from Merck Millipore). Differentiated PLB-985 cells stay in suspension and have neutrophil-like properties (Suppl. Mat. 14).

Beads. 20-µm and 8-µm diameter polystyrene microbeads at 10^6 beads/mL (Sigma-Aldrich) were washed three times by centrifugation at 16000 g for 3min and re-suspended in Dulbecco's Phosphate Buffered Saline (DPBS, Gibco) filtered with 0.22 µm diameter-pores (Merck Millipore). Beads were then incubated overnight at room temperature with 5% (w/v) Bovine Serum Albumin (BSA, Sigma-Aldrich) in DPBS. Beads were washed again three times by centrifugation at 16000 g during 3min, re-suspended in DPBS, and incubated with 1:500 anti-BSA rabbit antibody (Sigma-Aldrich, ref. B1520) in DPBS for an hour at room temperature. These IgG-coated beads were washed three times by centrifugation at 16000g for 3 min with DPBS and resuspended in DPBS at 10^6 beads/mL before use. Control beads were uncoated polystyrene beads, inducing very rare cases of adhesion with the cell but no phagocytosis. PLB cells tried almost systematically to internalize 20-µm activating beads by performing frustrated phagocytosis, and phagocyted 8-µm activating beads.

Atomic Force Microscope and Single Cell Force Spectroscopy

Cells and reagents. 3A9m T cells were obtained from D. Vignali (46) and cultured in RPMI completed with 5 % FBS, 10 mM Hepes, 10mM Sodium Pyruvate in 5 % CO2 atmosphere. COS-7 APCs were generated as previously described (47) by stably co-expressing the α and the β chains of the mouse MHC class II I-Ak , cultured in DMEM (5 % FBS, 1mM Sodium Pyruvate, 10 mM Hepes, and geneticin 10µg/ml). Cells were passaged up to three times a week by treating them with either Trypsin/EDTA or PBS 1X (w/o Ca2+/Mg2+), 0.53mM EDTA at 37°C for up to 5 min.

The anti CD45 antibodies used for this study were produced from the hybridoma collection of CIML, Marseille, France (namely H193.16.3)(48). Briefly, cells were routinely grown in complete culture medium (DMEM, 10% FBS, 1mM sodium pyruvate) prior to switching to the expansion and production phase. Hybridoma were then cultured in DMEM with decreasing concentrations of low immunoglobulin fetal bovine serum down to 0.5%. Cells were then maintained in culture for 5 additional days enabling immunoglobulin secretion prior to supernatant collection and antibody purification according to standard procedures.

The expression of TCR and CD45 molecules on T cells and MHC II molecules on COS-7 APC was assessed once a week by flow cytometry (anti-TCR PE clone H57.597, anti-CD45 Alexa Fluor 647 clone 30F11 were purchased from BD Pharmingen). The count and the viability, with Trypan blue, were assessed automatically twice by using Luna automated cell counter (Biozym Scientific). Mycoplasma test was assessed once a month. Culture media and PBS were purchased from Gibco (Life Technologies). PP2 (Lck inhibitor) was purchased from Calbiochem.

Substrates. Culture treated, sterile, glass bottom Petri dishes (World Precision Instruments Fluorodish FD35-100) were incubated with 50µg/ml anti-CD45 antibody for 1 hour at room temperature. The surfaces were extensively washed with PBS 1X prior to a last wash with HBSS 1X 10 mM Hepes. The surfaces were kept wet with HBSS 1X 10 mM Hepes before seeding T cells.

T cell preparation. T cells were counted, centrifuged and resuspended in HBSS 1X 10 mM Hepes and were kept for one hour at 37 °C 5% CO2 for recovery prior to seeding. The cells were seeded at room temperature and after 30 minutes a gentle wash was done by using two 1mL micropipettes in order to maintain, as much as possible, a constant volume in the Petri dish and hence avoid perturbations by important flows. After one hour incubation the Petri dish was mounted in a Petri dish Heater system (JPK Instruments) to maintain the temperature of the sample at ~ 37°C. 10 minutes before experiments, 10µM (final concentration) of Lck kinase inhibitor, PP2 drug was added and homogenized in the sample. We kept this drug present all along the experiments.

COS-7 APC preparation. The day before the experiment, COS-7 expressing MHCII cells were incubated with the peptide of interest with a final concentration of 10µM allowing 100% occupation of MHC II

molecules. Before the experiment the cells were detached from the cell culture plates by removing the cell medium, washed once with PBS 1X and then by a 0.53 mM EDTA treatment for 5 minutes at 37°C 10% CO2. The cells were resuspended in HBSS 1X 10mM Hepes and were allowed to recover before to be seeded into the sample. The peptide p46.61 (which is CD4 dependent) was purchased from Genosphere with a purity >95%.

AFM setup. The setup has been described in great detail elsewhere (49). Measurements were conducted with an AFM (Nanowizard I, JPK Instruments, Berlin) mounted on an inverted microscope (Zeiss Axiovert 200). The AFM head is equipped with a 15 µm *z*-range linearized piezoelectric scanner and an infrared laser. The set-up was used in closed loop, constant height feedback mode (36). MLCT gold-less cantilevers (MLCT-UC or MLCT-Bio DC, Bruker) were used in this study. The sensitivity of the optical lever system was calibrated on the glass substrate and the cantilever spring constant by using the thermal noise method. Spring constant were determined using JPK SPM software routines *in situ* at the start of each experiment. The calibration procedure for each cantilever was repeated three times to rule out possible errors. Spring constants were found to be consistently close to the manufacturer's nominal values and the calibration was stable over the experiment duration. The inverted microscope was equipped with 10x, 20xNA0.8 and 40xNA0.75 lenses and a CoolSnap HQ2 camera (Photometrics). Bright field images were used to select cells and monitor their morphology during force measurements through either Zen software (Zeiss) or Micro-Manager (39).

APC/T cell force measurements. *Lever decoration.* To make the cantilevers strongly adhesive, we used a modified version of our previous protocols (50). Briefly, cantilevers were activated using a 10 min residual air plasma exposure then dipped in a solution of 0.25mg/mL of Wheat Germ Agglutinin (WGA) or 0.5 mg/mL of Concanavalin A (ConA) in PBS 1x for at least one hour. They were extensively rinsed by shaking in 0.2µm filtered PBS 1x, stored in PBS 1x at 4°C. Before being mounted on the glass block lever holder, they were briefly dipped in MilliQ-H_2O in order to avoid the formation of salt crystals in case of drying and hence alteration of the reflection of the laser signal. *APC capture.* In separate experiments, we used side view and micropipette techniques, and we observed that (i) this allows the presented cell to be larger than the lever tip, excluding any unwanted contact of T cell with lectins and (ii) the binding is resistant enough to ensure that any rupture event recorded is coming from the cell/cell interface (Suppl. Mat. 3, Suppl. Fig. S2). After calibration, a lectin-decorated lever is pressed on a given COS7 cell for 20 to 60 seconds with a moderate force (typically 1-2nN), under continuous transmission observation. Then, the lever is retracted far from the surface and the cell is let to recover and adhere/spread for at least 5 minutes before starting the experiments (Suppl. Fig. S2). *SCFS experiment.* The surrogate APC is then positioned over a desired T cell. Because the lever is not coated with gold, hence almost transparent, one can finely position the probe over the target. Force curves are then recorded using the following parameters: max contact force 1nN, speeds 2µm/sec, acquisition frequency 2048 Hz, curve length 10µm and contact time 60 sec. At the end of the retraction, lateral motion of the cells is made by hand by moving the AFM head in the (x,y) plane, relative to the Petri dish substrate, until no more force is recorded by the lever, signaling that full separation was achieved (Suppl. Fig. S2). One APC cell was used to obtain one force curve on at least three different T cells, and 3 APCs at least were used for each condition. No apparent bias was detected in the data when carefully observing the succession of the measures for a given APC, for a given lever and for a set of T cells. *Data processing & Statistics.* Force curves were analyzed using JPK Data Processing software on a Linux 64 bits machine. Each curve was evaluated manually, except for calculation and plotting of mean±SD for relaxation curves where *ad-hoc* python scripts were used. Data were processed using Graphpad Prism (v7) on a Windows 7 machine. On graphs, data are presented as scatter dot plots with median and interquartile range. A data point corresponds to a force curve obtained for a given couple T cell/APC, except for the small detachment events where one data point corresponds to one such event (all events were pooled). Significance was assessed using Mann-Whitney tests in GraphPad Prism v7 with $p<0.05$ *, <0.01 **, <0.001 ***, and **** below; not significant otherwise.

Results

Micropipette rheometer for monitoring rapid morphological and mechanical changes in non-adherent cells

We implemented a real-time feedback loop in our Micropipette Force Probe setup (17, 33)(Fig. 1a) allowing us to impose a controlled small oscillatory force modulation $\Delta F cos(\omega t)$ (angular frequency $\omega = 2\pi f$, frequency f = 1 Hz) superimposed onto a constant force $\langle F \rangle$. A total force $F(t) = \langle F \rangle + \Delta F cos(\omega t)$ is thus applied to the leukocyte during its activation following the contact with an activating microbead coated with cell-specific antibodies. The contact is ensured by pressing the bead against the cell with a force F_{comp} (0.12-0.36 nN). This initial compression, from which we extract the cell's effective Young's modulus E_{Young} (51, 52) (Fig. 1b, inset, bottom right, and Suppl. Mat. 4), is followed by an imposed force modulation regime, where we measure oscillations in the position of the tip of the flexible micropipette $x_{tip}(t) = \langle x_{tip} \rangle + \Delta x_{tip} cos(\omega t - \varphi)$, of average value $\langle x_{tip} \rangle$, amplitude Δx_{tip}, (typically 100 nm, with a few-nanometer accuracy) and phase lag φ. Changes in $x_{tip}(t)$ reflect changes in cell length (Fig. 1b). As the cell is shorter when the force is higher, $x_{tip}(t)$ decreases when $F(t)$ increases, and corresponds to the lag between a maximum of the force and the following minimum of $x_{tip}(t)$ (Fig. 1b, inset, bottom right). From $x_{tip}(t)$ and $F(t)$, we deduce the complex cell stiffness $K^* = K' + iK''$, of elastic part $K' = \frac{\Delta F}{\Delta x_{tip}} \cos\varphi$ and viscous part $K'' = \frac{\Delta F}{\Delta x_{tip}} \sin\varphi$ (Suppl. Mat. 5, Suppl. Movie S1). We validated our setup by quantifying K^* of red blood cells (suppl. movie S2). We obtained values of K' very consistent with values predicted by existing models, and also obtained, as expected, very low values of K'' (Suppl. Mat. 6).

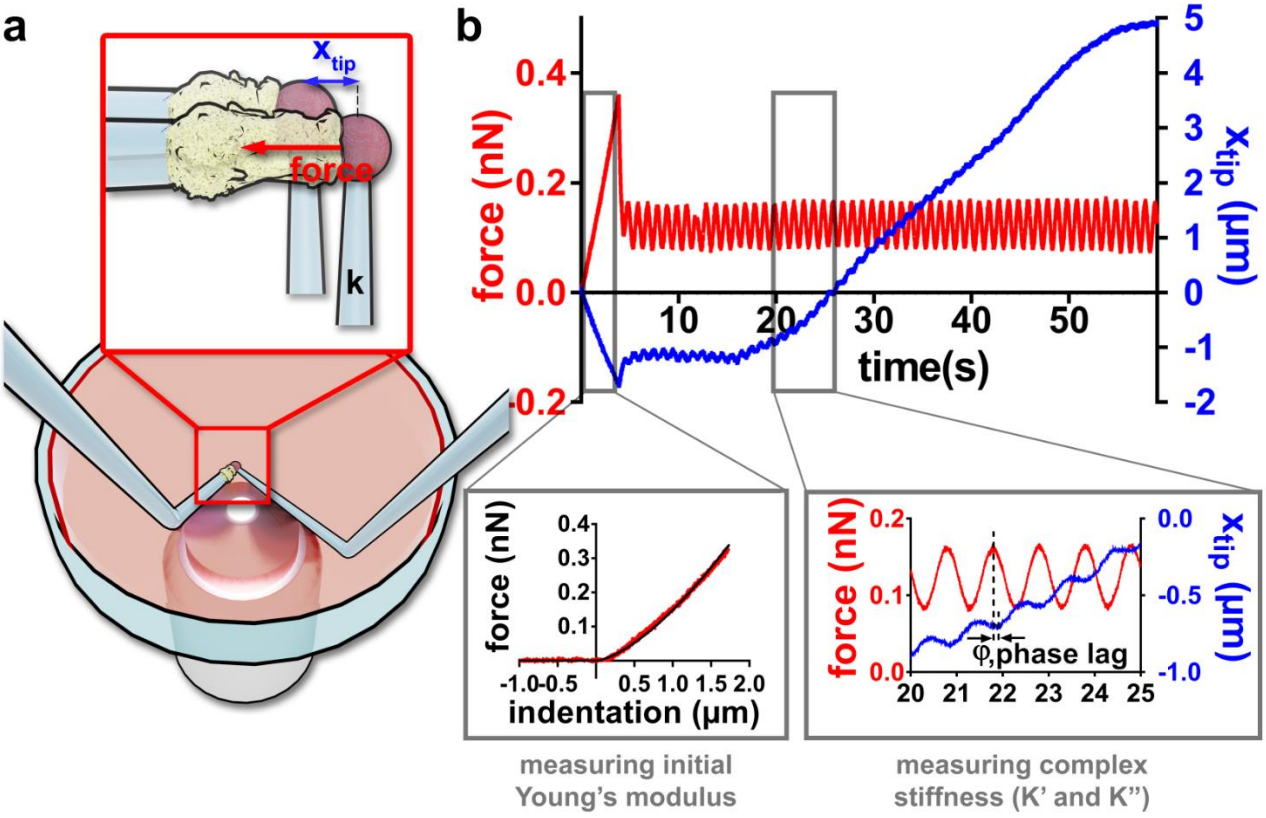

FIGURE 1. Rheological measurements during leukocyte activation. (**a**). Setup. Two micropipettes are plunged in a Petri dish. A flexible pipette (right, bending stiffness k≈0.2 nN/µm) holds an activating microbead firmly. A rigid micropipette (left) gently holds a leukocyte (aspiration pressure of 10-100 Pa). The base of the flexible micropipette is displaced to impose a desired force on the cell. (**b**) Force applied on the cell (in red) and the position x_{tip} of the tip of the flexible micropipette (in blue). The cell is first compressed with a force F_{comp} (here 0.36 nN) to measure the initial Young's modulus of the cell (inset, bottom left). Then an oscillatory force is applied to the cell,

leading to an oscillatory x_{tip} signal (inset, bottom right) superimposed to a slower variation of the average value $<x_{tip}>$ due to the growth of a protrusion produced by the leukocyte.

Leukocytes become stiffer and more viscous during activation

We probed three different types of leukocytes during their specific activation and observed qualitatively similar behavior: both *K'* and *K''* increase and reach a maximum that is 3- to 8-fold larger than their initial value within few minutes (~2 minutes for T and B cells, ~5 minutes for neutrophils-like PLB985 cells) following the contact between the leukocyte and the relevant activating microbead (Fig. 2, Suppl. Movie S1). The increase of *K'* and *K''* is in clear contrast with the constant values obtained using control non-activating beads (black lines on Fig. 2). Yet it is worth mentioning that the initial value of *K'* and *K''* is higher for activating beads than for control beads for T and B cells. We explain this by the fact that the initial time point for *K'* and *K''* is actually already ~10 seconds after initial cell-bead contact, leaving some time for early mechanical changes to occur (see later regarding mechanical changes). We evaluated the effect of temperature in the case of T cells by performing experiments at 37°C. T cells behaved qualitatively the same at 37°C, but reacted faster, and reached higher levels in *K'* and *K''* (Suppl. Mat. 7).

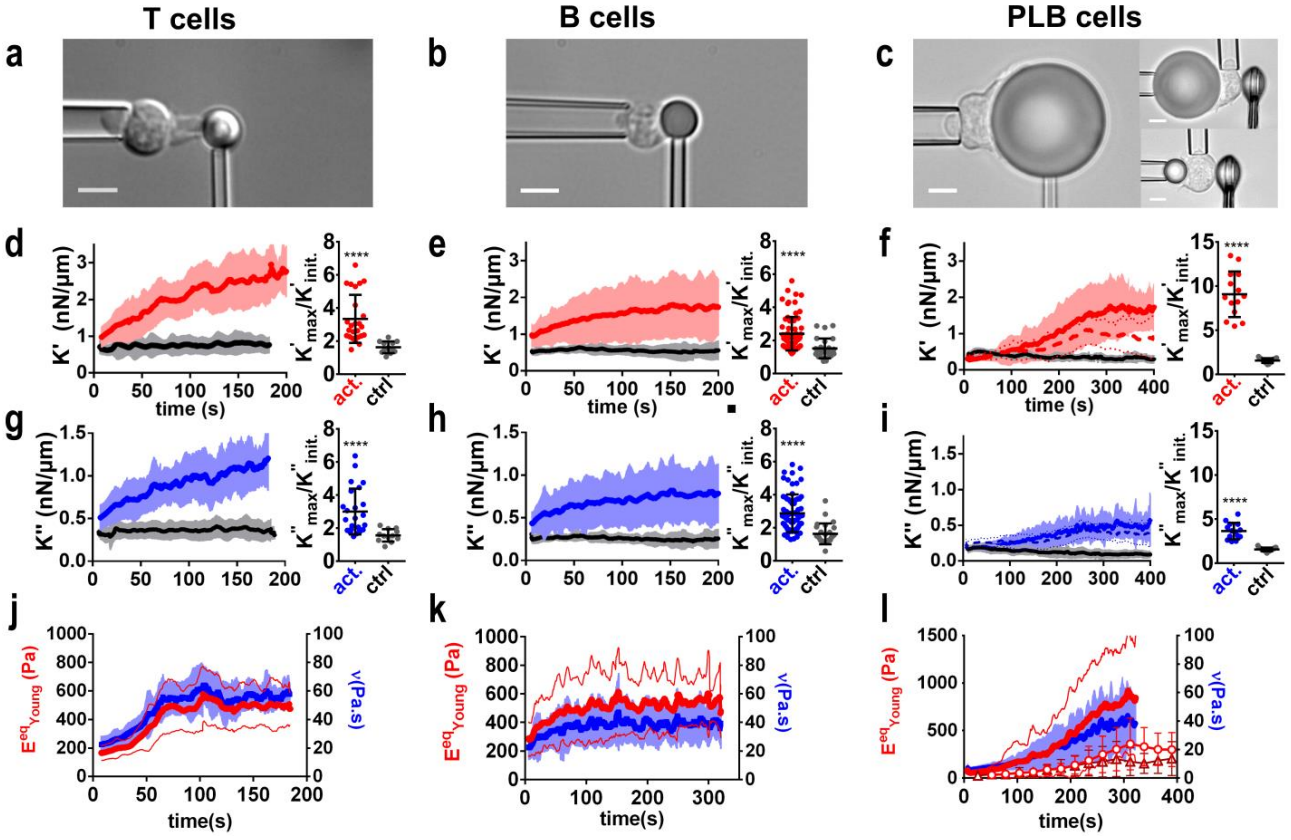

FIGURE 2. Both *K'* and *K''* increase during leukocyte activation. Each column corresponds to a different cell type. (**a-c**) Cell morphology. Scale bars are 5 µm. (**d-f**) Left: *K'* for activating (red lines) and non-activating control beads (gray lines). In **f,** solid red line is for 20-µm beads, dashed red line for 8-µm beads with indentation in the back (see Figure 3). Right: max/min ratio of *K'* values, for activating and non-activating control beads. (**g-i**) Left: *K''* values corresponding to *K'* values in **d-f**. In **i,** solid blue line is for 20-µm beads, dashed blue line for 8-µm beads with indentation in the back (see Figure 3). (**j-l**) Equivalent Young's modulus (red, left axis) and cell viscosity (blue, right axis). In **l,** dots are the Young's modulus measured in the back of the cell for 20-µm beads, triangles are for 8-µm beads . In all panels, leukocyte-bead contact time (t=0) is detected as a force increase, thick lines are mean±SD over at least 3 pooled experiments (T cells: 21 cells, B cells 71 cells, PLB cells: 14 cells). Mann-Whitney test, ****: p<0.0001.

Changes in *K'* and *K''* correspond to changes in intrinsic leukocyte mechanical properties

Both K' and K'' depend on cell geometry, so to exclude the possibility that changes in K' and K'' only reflect geometrical changes, cell intrinsic mechanical properties such as Young's modulus and viscosity have to be extracted from K' and K''. To do so, we first convert K' and K'' into a storage modulus E' and a loss modulus E'', respectively. In the case of T cells and B cells, we do so by modeling cell geometry (Suppl. Mat. 8).

For PLB cells, we use a modified setup where a non-adherent and non-activating glass bead indents the cell on its "back" (37) while the cell phagocytoses an activating bead at its "front" (Fig. 3a, Suppl. Movie S3) (37). This alternative setup leads to the same increase in K' and K'' as measured using the original setup with front indentation with an activating bead (Fig. 3b). Having a sphere-against-sphere geometry, we can use a linearized Hertz model to extract E' and E'' moduli (Suppl. Mat. 8). Lastly, we performed cyclic indentation experiments to measure directly the Young's modulus over time (with a limited time resolution of ~30 seconds, dotted curves in Fig. 2l): indentation occurs only for a short time at the beginning of each cycle, after which the indenter retracts from the cell, marking the end of a cycle, immediately followed by a new cycle (Suppl. Movie S4). In the case of PLB cells we tested the influence of bead size by performing indentation in the "back" of cells phagocytosing either 20- or 8-µm beads. For both bead sizes the cells' Young's modulus increased significantly during phagocytosis when comparing early (t=52 s) vs. late (t=286 s) times (Figure 2l, $E_{Young}(t = 286\ s) > E_{Young}(t = 52\ s)$, at least 14 cells from at least 3 independent experiments for each condition, $p<0.0001$ for 20-µm and 8-µm beads, Mann Whitney test).

To allow a simple interpretation of E' and E'', which were obtained in a regime of oscillatory forces, we convert them respectively into an effective Young's modulus E^{eq}_{Young} and an effective viscosity ν. To calculate E^{eq}_{Young}, we compare the Young's modulus measured by initial compression and E' measured right after, when force modulation begins (Suppl. Mat. 9; Suppl. Fig. S6). For PLB cells, we used again cyclic back-indentation as described above to measure both Young's modulus and E' not only at initial time but during the whole activation. This showed that E' and E_{Young} are proportional, with a phenomenological coefficient C such that $E' = CE_{Young}$. C is measured to be constant over time for PLB cells, and so for T and B cells we assume that C is also constant over time (Suppl. Mat. 9).

Using this approach, we measured the effective Young's modulus of the three cell types over time (Fig. 2j-l). To calculate the effective cell viscosity, we consider a simple model consistent with a Newtonian liquid and cortical tension model of a cell (2), where a Newtonian viscosity is introduced as $\nu = E''/\omega$. The resulting Young's modulus and viscosity increase until reaching a maximal value that is 2-3 fold higher than the baseline value for T and B cells, and about 11 fold higher for PLB cells (Fig. 2j-l).

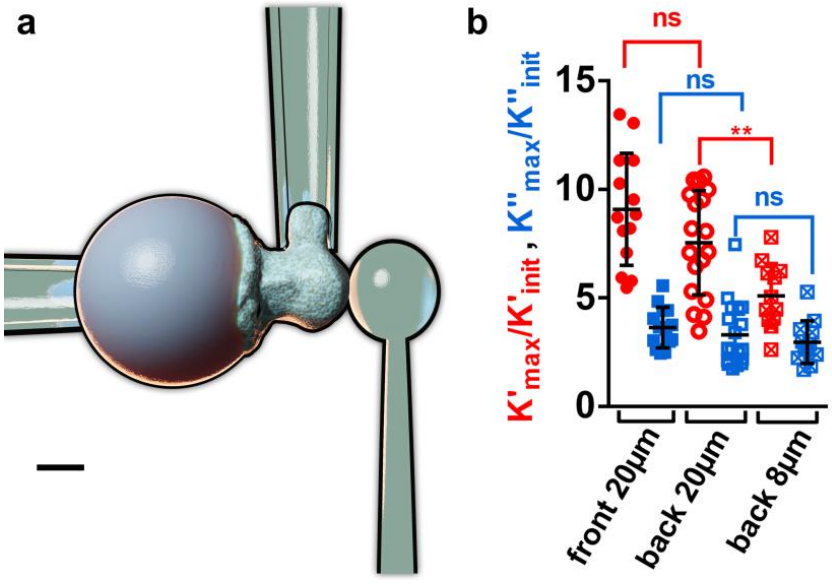

FIGURE 3. Indenting the "back" of a phagocyte during activation. (**a**) Modified setup. A stiff pipette holds the activating microbead (left), an auxiliary (stiff) pipette holds the cell by its "side" (top) and a flexible pipette whose tip consists of a non-adherent glass bead indents the cell on its "back" (right). Scale bar is 5 µm. (b) Max/min ratios for *K'* and *K''* obtained with both versions of the setup during PLB cell activation (ns: non-significant, two-tailed unpaired t test). Using back indentation, in addition to the 20-µm beads used with the non-modified setup, 8µm beads were tested.

Mechanical changes are localized close to the cell-bead interface

We asked if mechanical changes were localized close to the activation area in the leukocyte. In the case of T cells, we used a modified setup similar to the one allowing to indent PLB cells on their back (Fig. 3a). In that case an auxiliary pipette brought the activating microbead in contact with the T cell on its "side": at the equatorial plane (distance between the activating and indenting beads smaller than 5 µm), or close to the tip of the holding pipette, at the farthest possible location from the activating bead (distance between the activating and indenting beads larger than 5µm, Fig. 4, Suppl. Movie S5). This allowed us to quantify mechanical changes during activation depending on the distance to the cell-bead contact area. We computed an equivalent Young's modulus $E^{eq}{}_{Young}$ as described in supplementary material 9, which led to a good agreement with E_{Young} measured at the initial time. T cells exhibited a different behavior depending on the location of the activating microbead: the closer the indenter was to the activating bead, the larger the maximum value of $E^{eq}{}_{Young}$ measured during activation. Cell stiffening thus occurs with a different amplitude depending on the location on the cell relative to the contact zone with an activating surface.

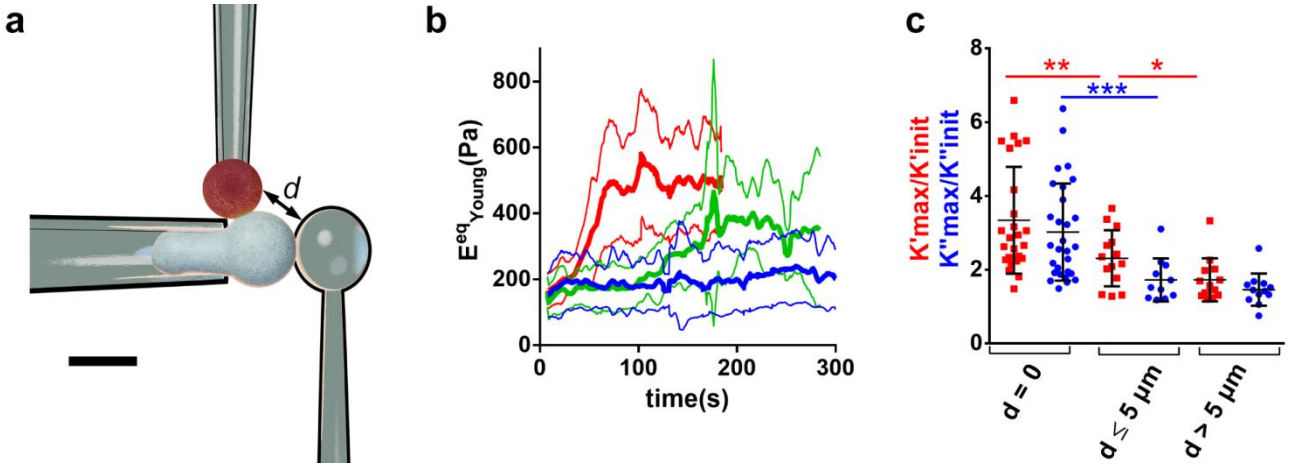

FIGURE 4. (**a**) Modified setup where an auxiliary (stiff) pipette holds the activating microbead (top, red) to bring it in contact with the T cell at a chosen distance from a microindenter (right), which indents the cell on its "side" while the T cell gets activated. Scale bar is 5 µm. (**b**) Equivalent Young's modulus for three different ranges of distance *d* between the activating bead and the microindenter (red: d=0; green: $0 < d \leq 5$ µm; blue: $d > 5$ µm). (**c**) K'_{max}/K'_{init} (red) and K''_{max}/K''_{init} (blue) ratios for the same ranges of distance *d* as in panel **b**.

Mechanical changes in T cells start within seconds

In T cells, mechanical changes precede morphological ones: *K'* increases slowly within seconds after cell-bead contact, before cell morphology starts changing (i.e. before the T cell produces a large protrusion (17), Suppl. Movie S1). The onset of this growth is followed by a short period during which *K'* stays relatively constant. This phase ends by a faster increase of *K'* during protrusion growth (Suppl. Mat. 10, Suppl. Fig. S7). The start of the faster increase in K' starts when the tail of the cell in the holding pipette starts retracting (a sign that *K'* and cell tension are two equivalent ways to describe cell stiffness, Suppl. Mat. 11). Of note, T cells have large membrane surface stores (38), so it is unlikely that the acceleration in *K'* increase could be explained by reaching the limits of membrane stores (Suppl. Mat. 12).

AFM measurements of early mechanical changes following T cell/APC contact

In order to confirm with an independent technique that T cell mechanics may be modulated within seconds when it encounters an antigen presenting cell (APC) before any large morphological change occurs, we used AFM and performed Single Cell Force Spectroscopy (SCFS) experiments (Fig. 5a, Suppl. Mat. 3)(36). As a model APC, we used COS-7 cells expressing MHCII molecules that can be loaded with peptides of desired affinity as previously shown (47, 48). We used murine 3A9m T cells and immobilized them on a coverslip by adhering them using anti-CD45 antibodies (53). To measure rapid mechanical changes using this technique, we prevented potential large active cell deformations by using the pan-Src kinase inhibitor PP2 (methods). Although PP2 inhibits TCR-mediated Lck- or Fyn- dependent intracellular phosphorylation events and downstream signaling cascades (54), it does not inhibit all molecular events such as migration arrest, kinapse or microcluster formation upon T cell activation (55–57). Washout experiment showed that PP2 in fact enables to pause signalization without abrogating the antigen dependence of early T cell activation (58, 59).

The SCFS experiments provide for each cell doublet the force-tip sample separation curve, which is the AFM equivalent of the force-indentation curve shown in Fig. 1b (inset, bottom left), with three parts : (i) pushing the cells together, (ii) maintaining the contact and (iii) detaching the cells by pulling them apart. The contact mechanics at initial time was quantified by measuring the slope of the force-tip sample separation curve (called contact slope herein), which reflects the stiffness of the cell doublet. This contact slope was not modified by the presence or absence on the APC of the HEL (Hen Egg Lysozyme, peptide p46.61)-derived peptide recognized by the murine 3A9m T cells (Supp. Fig. S2d). However, in the separation part of the force curves, the presence of the peptide induced an increase in the force needed to fully detach the two cells, in parallel of an increase of the number of discrete separation events, indicating that the interaction was indeed peptide specific (Suppl. Fig. S2e-f).

The measurement of the contact slope corresponds to the very first instants of cell-cell contact (Fig. 5a, bottom). To measure cell mechanical changes following this contact, we quantified the force relaxation when the AFM lever motion was stopped and piezo position was kept constant after reaching a contact force of 1nN (Fig. 5b-c). We observed a striking difference in this force relaxation depending on the presence *vs.* absence of a saturating concentration of the antigenic peptide (Fig. 5b): the force relaxation was much slower in presence of the antigenic peptide, as quantified by the lower value of the ratio $\Delta F/F_0$ at different times following the start of the relaxation (Fig. 5c). This measurement reflects global viscoelastic properties of the cell-cell doublet, but does not disentangle elastic and viscous properties. Furthermore, having the two cells pressed against each other in series does not allow simply excluding a contribution of a mechanical change in the APC. However, mechanical properties of APC COS-7 cells were not modified by the presence of the peptide (Suppl. Fig. S3). As a consequence, we expect that the major contribution to the difference in force relaxation is indeed due to the T cell. Our SCFS experiments are thus consistent with our Micropipette Force Probe experiments, and show that specific recognition during T cell/APC contact may induce mechanical changes, within few seconds, and without any TCR signaling.

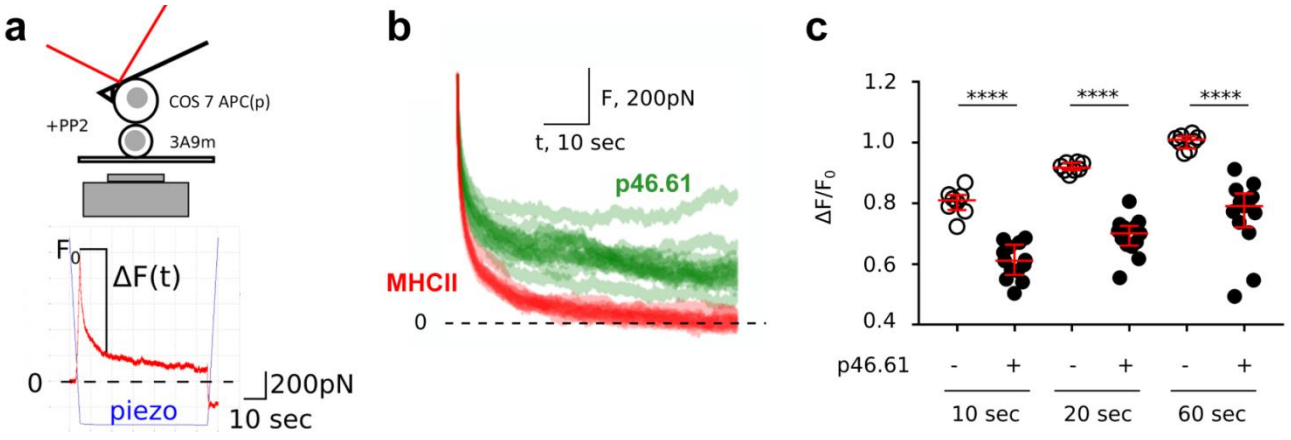

FIGURE 5. Cell-cell presentation induces early changes in force relaxation. (**a**) AFM SCFS Setup (top) and example of individual force (in red) vs. time curve (bottom). The piezo signal (in blue) reports the position of the base of the cantilever. (**b**) Relaxation part of force curves, for peptide (p46.61) *vs.* no-peptide (MHCII) cases. One curve corresponds to one cycle, ie. 1 APC/T cell couple. See Suppl. Fig. S2h for plot of mean±SD curves. (**c**) Quantification of the relaxation for three different time points, for MHCII (-) and MHCII/p46.61 (+); $\Delta F/F_0$ is the ratio of the drop in force ΔF and the force level F_0 imposed at initial time 0 (see **a**). This ratio is shown at three different time following cell-cell contact: 10, 20, and 60s, and shows a consistent lower ratio (hence a slower relaxation) in presence of the peptide (**** for p<0.001).

Relationship between elastic and viscous properties during leukocyte activation

We then asked if variations in elastic and viscous properties were related to each other. Prior works show that in several cell types the loss modulus E'' and storage modulus E' of a cell are related to each other. In fact their ratio $\eta = \frac{E''}{E'}$, the loss tangent, lies within a narrow range of 0.1-0.3(6, 28, 31, 60–62). For a material such as a purely viscous liquid, the storage modulus vanishes so that η is arbitrarily large, while for a purely elastic material, the loss modulus vanishes and so does η. A finite and constant value of η for a cell implies that the stiffer the cell, the more viscous it is. This narrow range of loss tangent is consistent with the conserved ratio of cortical tension to cell viscosity in leukocytes (see introduction). In biological matter, similar to soft glassy materials (63, 64), stress relaxation over time often follows a power-law (with an exponent that we shall call α)(31, 32, 60, 65, 66). The loss tangent η is frequency-dependent, and is expected to be approximately equal to $tan\left(\frac{\pi}{2}\alpha\right)$ at low frequencies (Suppl. Mat. 13). Therefore, by measuring the power-law exponent α independently, we should recover the value of $\eta = \frac{E''}{E'}$ (which should also be equal to $\frac{K''}{K'}$ as the contribution from geometry is eliminated in this ratio(7)). To test this prediction, we performed stress relaxation experiment on resting PLB cells (Fig. 6c) and obtained values for α that were very consistent with the predicted value of $\frac{2}{\pi} arctan\left(\frac{K''}{K'}\right)$ (which is equivalent to comparing $tan\left(\frac{\pi}{2}\alpha\right)$ and $\frac{K''}{K'}$, gray circle in Fig. 6b). We then compared *K'' vs. K'* curves obtained during activation of T cells, B cells, and PLB cells (Fig. 6a). In Figure 6b we plot the corresponding value of $\alpha = \frac{2}{\pi} arctan\eta = \frac{2}{\pi} arctan\frac{K''}{K'}$: these curves are remarkably consistent for T and B cells; for PLB cells, *K''-K'* curves obtained by indentation in the front and in the back of the cell are very similar, and differ from the T and B cell common curve. Interestingly, Bufi *et al.* (67) measured storage and loss moduli of various leukocytes at resting state or after priming by different inflammatory signals. Their data lead to a loss tangent η consistent with our measurements (Fig. 6d) but their measurements were made at a single time point. Maksym *et al.* (6) tracked over time both the loss and storage moduli of human airway smooth muscle cells contracting due to administration of histamine (Fig. 6d, inset, top left). Their data are again very consistent with our measurements. Roca-Cusachs *et al.* (2) used AFM on neutrophils, and found a loss tangent very consistent with our measurements on PLB cells obtained with 20-µm and 8-µm beads (Fig. 6d, inset, top right).

Based on our results, we propose a simple model of leukocyte mechanical changes during activation (Fig. 6e): mechanical changes begin seconds after receptor engagement at the leukocyte surface. Cell morphological changes start a few tens of seconds later, concomitant with stiffening and increase in viscosity. Viscous and elastic properties of the leukocyte evolve following a characteristic relationship defined by the loss tangent.

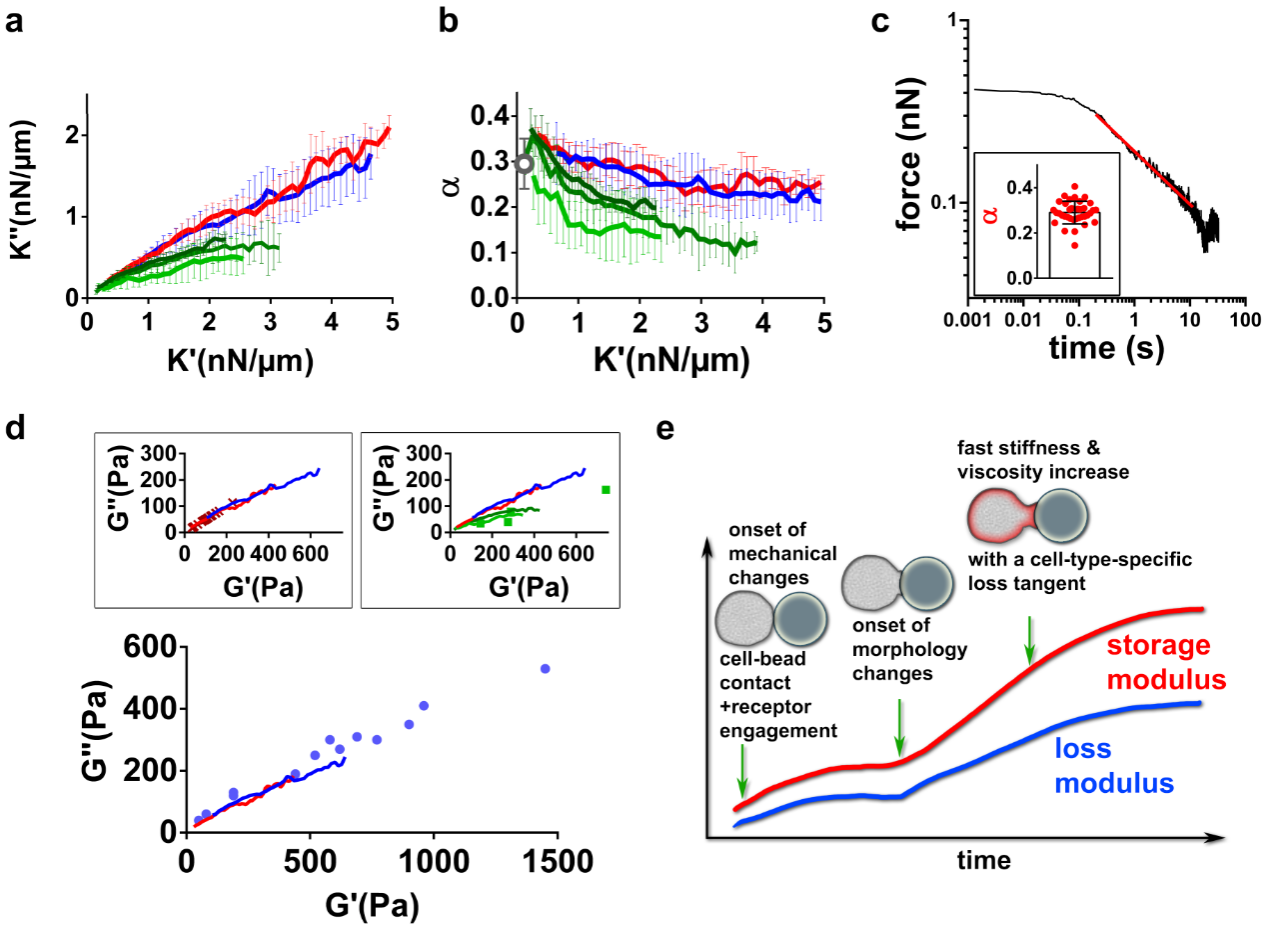

FIGURE 6. Relationship between elastic and viscous cell properties (**a**) *K'' vs. K'* during activation of T cells (red), B cells (blue) and PLB cells (front indentation: green (20-μm beads), back indentation: light green (20-μm beads) and dark green (8-μm beads)). Error bar are SDs. (**b**) $\alpha = \frac{2}{\pi} arctan\left(\frac{K''}{K'}\right)$ corresponding to the same data as in **a**. The gray circle is the value of the power-law exponent in force relaxation experiments on resting PLB cells. (**c**) Example of force relaxation curve of a PLB cell. In the log-log plot, a power-law relaxation is identified by the straight line (red), whose slope is the exponent α. Inset: individual α values (1 dot per cell). (**d**) Loss modulus *G''* *vs.* storage modulus *G'* obtained by Bufi *et al.*(67) (bottom, blue dots), Maksym *et al.*(6)(inset, top left, red crosses), and Roca-Cusachs *et al.*(2) (inset, top right, green dots). Our data from **a** (red and blue solid lines) are consistent with the above-mentioned published data. (**e**) Proposed model of mechanical changes during leukocyte activation.

Discussion

We showed that during activation, various types of leukocytes see their stiffness and viscosity increase significantly within few minutes. The initiation of mechanical changes upon contact with an activating surface starts within seconds and these changes precede morphological changes. By using the same technique – avoiding potential differences due to different techniques (3) – we show to our knowledge for the first time with ~1-s time resolution how both viscous and elastic properties evolve during immune cell activation. We further show that elastic and viscous properties follow a relationship that is cell-type dependent: T and B cells keep the same ratio between viscous and elastic properties, while neutrophils follow a different ratio, independently of the size of their target.

Most published measurements of cell viscosity were performed on leukocytes in a resting state. Some micropipette aspiration studies led to leukocyte viscosity in the range of 100-200 Pa.s (68–71), and are consistent with values obtained in fibroblasts (72). These values are higher than the viscosities of ~5-20 Pa.s that we measured in resting leukocytes. This discrepancy might be explained by model-dependence and by differences in the shear rate applied to cells. Our measurements are much

closer to results by other groups: Sung *et al.* (73) obtained a cytotoxic T cell viscosity of ~30 Pa.s, Schmid-Schönbein *et al.* (25) measured a leukocyte viscosity of ~13 Pa.s, Hochmuth *et al.* (29) extrapolated a value for neutrophil viscosity of ~ 60 Pa.s. Interestingly, Lipowsky *et al.* (74) did not restrict to baseline viscosity and studied neutrophils stimulated by the chemoattractant FMLP. The authors reported a neutrophil viscosity increasing from ~5 Pa.s at resting state to ~70 Pa.s upon stimulation.

Mechanical changes might not have a function *per se*, but might be concomitant to force generation by cells. Indeed, cell contractility and cell stiffness are correlated in muscle cells (75–79), and single cells mirror mechanical and energetic features of muscle contraction: single myoblasts follow a single-cell equivalent of a Hill relationship between force generation and rate of contraction (80, 81). Furthermore, it also appears that single muscle cells become stiffer when they contract: Shroff et al. (79) observed a roughly 2-fold increase in stiffness of a cardiomyocyte during its contraction. Although leukocytes have a different organization of their actomyosin cytoskeleton, it is tempting to speculate that all leukocytes share generic cytoskeletal-based properties requiring that cells stiffen to generate force. This could explain the apparent contradiction that in leukocytes, the stiffening that we have quantified occurs in situations requiring an efficient spreading. Indeed, phagocytes need to increase their surface by spreading on their prey to engulf it, while T and B cells need to spread widely on the cell they encounter to quickly scan a surface that is as large as possible on the cell they interact with (18, 82). Alternatively, forming a stiff synapse might allow its stabilization (83, 84).

Although the molecular details leading to changes in viscoelastic properties are yet to be understood, cell-scale physical considerations allowed Evans et al. (71, 85) to conclude that viscous properties of cells are conferred by bulk components of the cell, as opposed to surface viscosity due to the actin cortex. As a result, we expect that the large increase in viscous properties of leukocytes that we observed are largely due to intracellular reorganization, not only to cortical reorganizations. Interestingly, Tsopoulidis *et al.* recently showed that T cell receptor engagement triggers the formation of a nuclear actin network in T cells (86), which could contribute to these bulk mechanical changes. Fritzsche *et al.* observed submembrane actin pattern reorganization that influenced the membrane architecture of Hela cells, but not their mechanical properties (87). These observations may lift an apparent contradiction in T cells, in which the formation of a immunological synapse requires actin to depolymerize at the center of the synapse, including in cytotoxic T cells where actin gets actually depleted across the synapse within 1 min (88). Other contributors must then explain the stiffening that we observe, and in addition to the nuclear actin network (86), another possible contributor being a secondary actin network. Indeed Fritzsche et al. (84) found in T cells that beside the dense cortical network forming a rosette-shaped structure in the basal lamellipodium and devoid of actin at its center up to 3 min after initial contact, another actin network assembles 150 to 300 nm above the cell-substrate contact.

We expect inner reorganizations causing mechanical changes to impact inner cell dynamics, such as organelle trafficking. This includes mitochondrial relocation that is known to happen in several types of leukocytes upon activation (89, 90). Regarding cell surface, although we dismissed surface effects as key contributors to cell viscosity, surface receptors are transmembraneous so that the formation of diffusional barriers with slowed diffusion at the cell surface as observed during leukocyte activation could be one manifestation of the increase in cell viscosity (91, 92). As an alternative to the above considerations that mechanical changes might not have a specific function, these changes in viscosity might help confining molecules of interest in the vicinity of the synapse. By sequestering these molecules due to higher stiffness and viscosity (implicating an increased energetical cost to move away from this zone), early mechanical changes might help integrating at the cellular scale the information input incoming from the single-receptor scale at the synapse. Considering this efficient processing from nano- to micro-scale is also worth integrating in mechanistic description of early immunological signaling, including models considering a frictional coupling of the TCR to the cytoskeleton (93, 94).

Our study highlights that variations of both elastic and viscous properties are relevant to understand immune cell mechanics during activation, as well as their relationship in the form of the loss

tangent η, and how the latter evolves over time. All the leukocytes that we tested show very large changes in both elastic and viscous properties, but monitoring the time evolution of the loss tangent exhibits a mechanical fingerprint specific to cell types. It is tempting to speculate that the evolution of the loss tangent during activation can become a valuable tool to discriminate between healthy and pathological leukocytes as already suggested by considering static values of η (95).

Finally, our observations suggest a possible generalization to cells other than leukocytes. In line with what was observed by Thoumine et al. (96) in fibroblasts or Abidine et al. in epithelial cancer cells (97), we propose that getting stiffer and more viscous while spreading is a common behavior across cell types. The time evolution of the loss tangent during cell spreading remains to be explored.

Author contributions

P.-H.P., Y.H. and J.H. designed experiments; A.Z., S.V.M.C., A.S., F.M., Y.H., P.-H.P. and J.H. performed experiments; A.Z., A.S., Y.H., P.-H.P. and J.H. analyzed the data; A.B., S.D., E.H., S.D.-C., H.-T.H., A.I.B., Y.R.C., Y.H., C.H. and O.N. contributed material; P.-H.P. and J.H. wrote the manuscript with helpful critical reading by the other authors.

Competing financial interests

The authors declare no competing financial interests.

Acknowledgements

This work has benefited from the financial support of the LabeX LaSIPS (ANR-10-LABX-0040-LaSIPS) managed by the French National Research Agency under the "Investissements d'avenir" program (n°ANR-11-IDEX-0003-02), from a CNRS PEPS grant, from Ecole Polytechnique, and from an endowment in cardiovascular bioengineering from the AXA Research Fund. This work was supported by funding from (a) Prise de Risques CNRS and ANR JCJC « DissecTion » (to PHP) ; (b) the Labex IN-FORM (ANR-11-LABX-0054) and A*MIDEX project (n° ANR-11-IDEX-0001-02), sponsored by the Investissements d'Avenir project funded by the French Government, managed by the French National Research Agency (ANR) (to LAI & CIML, and as PhD grant to AS) ; (c) the European Union's Horizon 2020 research and innovation programme under the Marie Skłodowska-Curie grant agreement No713750, with the financial support of the Regional Council of Provence- Alpes-Côte d'Azur and with of the A*MIDEX (n° ANR- 11-IDEX-0001-02), funded by the Investissements d'Avenir project funded by the French Government, managed by the French National Research Agency (ANR) (as PhD grant to FM). Part of this work was also supported by institutional grants from INSERM, CNRS and Aix-Marseille University to the LAI and CIML. Material or technical help: R. Balland (Sensome) for RBCs; M. Pélicot-Biarnes (LAI); L. Borge (PCC cell culture facility); S. Mailfert / M. Fallet / PICSL imaging facility of the CIML (ImagImm), member of the national infrastructure France-BioImaging supported by the French National Research Agency (ANR-10-INBS-04); A. Formisano (He/Marguet lab). Discussion and support: D. Gonzalez-Rodriguez (LCP-A2MC, Univ. De Lorraine), R Roncagalli (CIML); P. Recouvreux (IBDML); L. Limozin, F. Rico (LAI). Companies: F. Eghiaian, T. Plake & JPK Instruments (Berlin, Germany), now part of Bruker, for continuous support and generous help; Zeiss France for support. SVMC and YRC have benefited from the financial support of an FPI contract (BES-2014-068006) and the grant BFU2013-48828-P from the Spanish Ministry of Economy (MINECO).

References

1. Hochmuth, R.M. 2000. Micropipette aspiration of living cells. J. Biomech. 33: 15–22.
2. Roca-Cusachs, P., I. Almendros, R. Sunyer, N. Gavara, R. Farré, and D. Navajas. 2006. Rheology of Passive and Adhesion-Activated Neutrophils Probed by Atomic Force Microscopy. Biophys. J. 91: 3508–3518.
3. Wu, P.-H., D.R.-B. Aroush, A. Asnacios, W.-C. Chen, M.E. Dokukin, B.L. Doss, P. Durand-Smet, A. Ekpenyong, J. Guck, N. V. Guz, P.A. Janmey, J.S.H. Lee, N.M. Moore, A. Ott, Y.-C. Poh, R. Ros, M. Sander, I. Sokolov, J.R. Staunton, N. Wang, G. Whyte, and D. Wirtz. 2018. A comparison of

methods to assess cell mechanical properties. Nat. Methods. 15: 491–498.
4. Toepfner, N., C. Herold, O. Otto, P. Rosendahl, A. Jacobi, M. Kräter, J. Stächele, L. Menschner, M. Herbig, L. Ciuffreda, L. Ranford-Cartwright, M. Grzybek, Ü. Coskun, E. Reithuber, G. Garriss, P. Mellroth, B. Henriques-Normark, N. Tregay, M. Suttorp, M. Bornhäuser, E.R. Chilvers, R. Berner, and J. Guck. 2018. Detection of human disease conditions by single-cell morpho-rheological phenotyping of blood. Elife. 7: e29213.
5. Guillou, L., J.B.J.B. Dahl, J.-M.G.J.-M.G. Lin, A.I.A.I. Barakat, J. Husson, S.J.S.J. Muller, and S. Kumar. 2016. Measuring Cell Viscoelastic Properties Using a Microfluidic Extensional Flow Device. Biophys. J. 111: 2039–2050.
6. Maksym, G.N., B. Fabry, J.P. Butler, D. Navajas, D.J. Tschumperlin, J.D. Laporte, and J.J. Fredberg. 2000. Mechanical properties of cultured human airway smooth muscle cells from 0.05 to 0.4 Hz. J. Appl. Physiol. 89: 1619–1632.
7. Smith, B.A., B. Tolloczko, J.G. Martin, and P. Grütter. 2005. Probing the Viscoelastic Behavior of Cultured Airway Smooth Muscle Cells with Atomic Force Microscopy: Stiffening Induced by Contractile Agonist. Biophys. J. 88: 2994–3007.
8. Dura, B., S.K. Dougan, M. Barisa, M.M. Hoehl, C.T. Lo, H.L. Ploegh, and J. Voldman. 2015. Profiling lymphocyte interactions at the single-cell level by microfluidic cell pairing. Nat. Commun. 6: 5940.
9. Niedergang, F., V. Di Bartolo, and A. Alcover. 2016. Comparative Anatomy of Phagocytic and Immunological Synapses. Front. Immunol. 7: 1–9.
10. Hivroz, C., and M. Saitakis. 2016. Biophysical Aspects of T Lymphocyte Activation at the Immune Synapse. Front. Immunol. 7: 1–12.
11. Huse, M. 2017. Mechanical forces in the immune system. Nat. Rev. Immunol. 17: 679–690.
12. Wang, J., F. Lin, Z. Wan, X. Sun, Y. Lu, J. Huang, F. Wang, Y. Zeng, Y.H. Chen, Y. Shi, W. Zheng, Z. Li, C. Xiong, and W. Liu. 2018. Profiling the origin, dynamics, and function of traction force in B cell activation. Sci. Signal. 11.
13. Kumari, A., J. Pineau, P.J. Sáez, M. Maurin, D. Lankar, M. San Roman, K. Hennig, V.F. Boura, R. Voituriez, M.C.I. Karlsson, M. Balland, A.M. Lennon Dumenil, and P. Pierobon. 2019. Actomyosin-driven force patterning controls endocytosis at the immune synapse. Nat. Commun. 10: 1–14.
14. Evans, E., A. Leung, and D. Zhelev. 1993. Synchrony of cell spreading and contraction force as phagocytes engulf large pathogens. J. Cell Biol. 122: 1295–300.
15. Kumari, S., M. Mak, Y. Poh, M. Tohme, N. Watson, M. Melo, E. Janssen, M. Dustin, R. Geha, and D.J. Irvine. 2020. Cytoskeletal tension actively sustains the migratory T-cell synaptic contact. EMBO J. : 1–18.
16. Masters, T.A., M.P. Sheetz, and N.C. Gauthier. 2016. F-actin waves, actin cortex disassembly and focal exocytosis driven by actin-phosphoinositide positive feedback. Cytoskeleton. 73: 180–196.
17. Sawicka, A., A. Babataheri, S. Dogniaux, A.I. Barakat, D. Gonzalez-Rodriguez, C. Hivroz, and J. Husson. 2017. Micropipette Force Probe to quantify single-cell force generation: application to T cell activation. Mol. Biol. Cell. 28: mbc.E17-06-0385.
18. Herant, M., V. Heinrich, and M. Dembo. 2005. Mechanics of neutrophil phagocytosis: behavior of the cortical tension. J. Cell Sci. 118: 1789–97.
19. Irmscher, M., A.M. De Jong, H. Kress, and M.W.J. Prins. 2013. A method for time-resolved measurements of the mechanics of phagocytic cups. J. R. Soc. Interface. 10.
20. Merino-Cortés, S. V., S.R. Gardeta, S. Roman-Garcia, A. Martínez-Riaño, J. Pineau, R. Liebana, I. Merida, A.-M.L. Dumenil, P. Pierobon, J. Husson, B. Alarcon, and Y.R. Carrasco. 2020. Diacylglycerol kinase ζ promotes actin cytoskeleton remodeling and mechanical forces at the B cell immune synapse. Sci. Signal. 13: eaaw8214.
21. Ekpenyong, A.E., N. Toepfner, C. Fiddler, M. Herbig, W. Li, G. Cojoc, C. Summers, J. Guck, and E.R. Chilvers. 2017. Mechanical deformation induces depolarization of neutrophils. Sci. Adv. 3: e1602536.
22. Worthen, G.S.S., B.I. Schwab, E.L. Elson, G.P.G.P.G.P. Downey, B. Schwab 3rd, E.L. Elson, and G.P.G.P.G.P. Downey. 1989. Mechanics of stimulated neutrophils: cell stiffening induces retention in capillaries. Science. 245: 183.
23. Bashant, K.R., A. Vassallo, C. Herold, R. Berner, L. Menschner, J. Subburayalu, M.J. Kaplan, C. Summers, J. Guck, E.R. Chilvers, and N. Toepfner. 2019. Real-time deformability cytometry reveals sequential contraction and expansion during neutrophil priming. J. Leukoc. Biol. 105:

1143–1153.
24. Preira, P., J.-M. Forel, P. Robert, P. Nègre, M. Biarnes-pelicot, F. Xeridat, P. Bongrand, L. Papazian, O. Theodoly, P. Negre, M. Biarnes-pelicot, F. Xeridat, P. Bongrand, L. Papazian, and O. Theodoly. 2016. The leukocyte-stiffening property of plasma in early acute respiratory distress syndrome (ARDS) revealed by a microfluidic single-cell study: the role of cytokines and protection with antibodies. Crit. Care. 20: 8.
25. Schmid-Schönbein, G.G.W., K.K.L. Sung, H. Tözeren, R. Skalak, and S. Chien. 1981. Passive mechanical properties of human leukocytes. Biophys. J. 36: 243–256.
26. Evans, E.A. 1984. Structural model for passive granulocyte behaviour based on mechanical deformation and recovery after deformation tests. Kroc Found. Ser. 16: 53–71.
27. Tran-Son-Tay, R., D. Needham, A. Yeung, and R.M. Hochmuth. 1991. Time-dependent recovery of passive neutrophils after large deformation. Biophys. J. 60: 856–866.
28. Fabry, B., G.N. Maksym, J.P. Butler, M. Glogauer, D. Navajas, and J.J. Fredberg. 2001. Scaling the Microrheology of Living Cells. Phys. Rev. Lett. 87: 148102.
29. Hochmuth, R.M., H.P. Ting-Beall, B.B. Beaty, D. Needham, and R. Tran-Son-Tay. 1993. Viscosity of passive human neutrophils undergoing small deformations. Biophys. J. 64: 1596–601.
30. Lam, J., M. Herant, M. Dembo, and V. Heinrich. 2009. Baseline mechanical characterization of J774 macrophages. Biophys. J. 96: 248–54.
31. Alcaraz, J., L. Buscemi, M. Grabulosa, X. Trepat, B. Fabry, R. Farre, D. Navajas, R. Farré, and D. Navajas. 2003. Microrheology of Human Lung Epithelial Cells Measured by Atomic Force Microscopy. Biophys. J. 84: 2071–2079.
32. Mahaffy, R.E.E., S. Park, E. Gerde, J. Käs, and C.K.K. Shih. 2004. Quantitative analysis of the viscoelastic properties of thin regions of fibroblasts using atomic force microscopy. Biophys. J. 86: 1777–93.
33. Basu, R., B.M.B.M. Whitlock, J. Husson, A. Le Floc'h, W. Jin, A. Oyler-Yaniv, F. Dotiwala, G. Giannone, C. Hivroz, N. Biais, J. Lieberman, L.C.L.C. Kam, M. Huse, A. Le Floc'h, W. Jin, A. Oyler-Yaniv, F. Dotiwala, G. Giannone, C. Hivroz, N. Biais, J. Lieberman, L.C.L.C. Kam, and M. Huse. 2016. Cytotoxic T Cells Use Mechanical Force to Potentiate Target Cell Killing. Cell. 165: 100–110.
34. Husson, J., K. Chemin, A. Bohineust, C. Hivroz, and N. Henry. 2011. Force Generation upon T Cell Receptor Engagement. PLoS One. 6: e19680.
35. Zucchetti, A.E., N. Paillon, O. Markova, S. Dogniaux, C. Hivroz, and J. Husson. 2021. Influence of external forces on actin-dependent T cell protrusions during immune synapse formation. Biol. Cell. .
36. Puech, P.H., K. Poole, D. Knebel, and D.J. Muller. 2006. A new technical approach to quantify cell-cell adhesion forces by AFM. Ultramicroscopy. .
37. Guillou, L., A. Babataheri, P.-H. Puech, A.I. Barakat, and J. Husson. 2016. Dynamic monitoring of cell mechanical properties using profile microindentation. Sci. Rep. 6: 21529.
38. Guillou, L., A. Babataheri, M. Saitakis, A. Bohineust, S. Dogniaux, C. Hivroz, A.I. Barakat, and J. Husson. 2016. T-lymphocyte passive deformation is controlled by unfolding of membrane surface reservoirs. Mol. Biol. Cell. 27: 3574–3582.
39. Edelstein, A.D., M. a Tsuchida, N. Amodaj, H. Pinkard, R.D. Vale, and N. Stuurman. 2014. Advanced methods of microscope control using μManager software. J. Biol. Methods. 1: 10.
40. Larghi, P., D.J. Williamson, J.-M. Carpier, S. Dogniaux, K. Chemin, A. Bohineust, L. Danglot, K. Gaus, T. Galli, and C. Hivroz. 2013. VAMP7 controls T cell activation by regulating the recruitment and phosphorylation of vesicular Lat at TCR-activation sites. Nat. Immunol. 14: 723–731.
41. Roman-Garcia, S., S. V. Merino-Cortes, S.R. Gardeta, M.J.W. de Bruijn, R.W. Hendriks, and Y.R. Carrasco. 2018. Distinct roles for Bruton's Tyrosine Kinase in B cell immune synapse formation. Front. Immunol. .
42. Drexler, H.G., W.G. Dirks, Y. Matsuo, and R.A.F. MacLeod. 2003. False leukemia–lymphoma cell lines: an update on over 500 cell lines. Leukemia. 17: 416–426.
43. Romano, P., A. Manniello, O. Aresu, M. Armento, M. Cesaro, and B. Parodi. 2009. Cell Line Data Base: Structure and recent improvements towards molecular authentication of human cell lines. Nucleic Acids Res. .
44. Rincón, E., B.L. Rocha-Gregg, and S.R. Collins. 2018. A map of gene expression in neutrophil-like cell lines. BMC Genomics. 19: 573.
45. Pedruzzi, E., M. Fay, C. Elbim, M. Gaudry, and M.A. Gougerot-Pocidalo. 2002. Differentiation of

PLB-985 myeloid cells into mature neutrophils, shown by degranulation of terminally differentiated compartments in response to N-formyl peptide and priming of superoxide anion production by granulocyte-macrophage colony-stimulating fact. Br. J. Haematol. .
46. Vignali, D.A.A., and J.L. Strominger. 1994. Amino acid residues that flank core peptide epitopes and the extracellular domains of cd4 modulate differential signaling through the t cell receptor. J. Exp. Med. .
47. Salles, A., C. Billaudeau, A. Sergé, A.M. Bernard, M.C. Phélipot, N. Bertaux, M. Fallet, P. Grenot, D. Marguet, H.T. He, and Y. Hamon. 2013. Barcoding T Cell Calcium Response Diversity with Methods for Automated and Accurate Analysis of Cell Signals (MAAACS). PLoS Comput. .... 9: 24–26.
48. Hueber, A.O., M. Pierres, and H.T. He. 1992. Sulfated glycans directly interact with mouse Thy-1 and negatively regulate Thy-1-mediated adhesion of thymocytes to thymic epithelial cells. J. Immunol. .
49. Cazaux, S., A. Sadoun, M. Biarnes-pelicot, M. Martinez, M. Pélicot-Biarnes, M. Martinez, S. Obeid, P. Bongrand, L. Limozin, and P.H. Puech. 2016. Synchronizing atomic force microscopy force mode and fluorescence microscopy in real time for immune cell stimulation and activation studies. Ultramicroscopy. 160: 168–181.
50. Franz, C.M., A. Taubenberger, P.H. Puech, and D.J. Muller. 2007. Studying integrin-mediated cell adhesion at the single-molecule level using AFM force spectroscopy. Sci. STKE. .
51. Johnson, K.L. 1985. Contact Mechanics. J. Am. Chem. Soc. 37: 1–17.
52. Rosenbluth, M.J., W.A. Lam, and D.A. Fletcher. 2006. Force microscopy of nonadherent cells: a comparison of leukemia cell deformability. Biophys. J. 90: 2994–3003.
53. A. Sadoun , M. Biarnes-Pelicot , L. Ghesquiere-Dierickx A. Wu , O. Théodoly , L.Limozin, Y. Hamon, P.-H.P. 2020. Controlling T cells shape, mechanics and activation by micropatterning. bioRxiv. : 1–29.
54. Hanke, J.H., J.P. Gardner, R.L. Dow, P.S. Changelian, W.H. Brissette, E.J. Weringer, B.A. Pollok, and P.A. Connelly. 1996. Discovery of a novel, potent, and Src family-selective tyrosine kinase inhibitor: Study of Lck- and FynT-dependent T cell activation. J. Biol. Chem. .
55. Moreau, H.D., F. Lemaître, K.R. Garrod, Z. Garcia, A.-M.M. Lennon-Duménil, P. Bousso, and M.D. Cahalan. 2015. Signal strength regulates antigen-mediated T-cell deceleration by distinct mechanisms to promote local exploration or arrest. Proc. Natl. Acad. Sci. U. S. A. 112: 12151–12156.
56. Campi, G., R. Varma, and M.L. Dustin. 2005. Actin and agonist MHC-peptide complex-dependent T cell receptor microclusters as scaffolds for signaling. J. Exp. Med. 202: 1031–1036.
57. Yokosuka, T., K. Sakata-Sogawa, W. Kobayashi, M. Hiroshima, A. Hashimoto-Tane, M. Tokunaga, M.L. Dustin, and T. Saito. 2005. Newly generated T cell receptor microclusters initiate and sustain T cell activation by recruitment of Zap70 and SLP-76. Nat. Immunol. 6: 1253–62.
58. Faroudi, M., R. Zaru, P. Paulet, S. Müller, and S. Valitutti. 2003. Cutting Edge: T Lymphocyte Activation by Repeated Immunological Synapse Formation and Intermittent Signaling. J. Immunol. .
59. Osborne, D.G., and S.A. Wetzel. 2012. Trogocytosis Results in Sustained Intracellular Signaling in CD4 + T Cells . J. Immunol. .
60. Kollmannsberger, P., and B. Fabry. 2011. Linear and Nonlinear Rheology of Living Cells. Annu. Rev. Mater. Res. 41: 75–97.
61. Balland, M., N. Desprat, D. Icard, S. Féréol, A. Asnacios, J. Browaeys, S. Hénon, and F. Gallet. 2006. Power laws in microrheology experiments on living cells: Comparative analysis and modeling. Phys. Rev. E. 74: 021911.
62. Bursac, P., G. Lenormand, B. Fabry, M. Oliver, D.A. Weitz, V. Viasnoff, J.P. Butler, and J.J. Fredberg. 2005. Cytoskeletal remodelling and slow dynamics in the living cell. Nat. Mater. 4: 557–561.
63. Sollich, P. 1997. Rheological constitutive equation for model of soft glassy materials. Phys. Rev. E - Stat. Physics, Plasmas, Fluids, Relat. Interdiscip. Top. 58: 738–759.
64. Fabry, B., and J.J. Fredberg. 2003. Remodeling of the airway smooth muscle cell: are we built of glass? Respir. Physiol. Neurobiol. 137: 109–124.
65. Fabry, B., G.N. Maksym, J.P. Butler, M. Glogauer, D. Navajas, N.A. Taback, E.J. Millet, and J.J. Fredberg. 2003. Time scale and other invariants of integrative mechanical behavior in living cells. Phys. Rev. E - Stat. Physics, Plasmas, Fluids, Relat. Interdiscip. Top. 68: 1–18.

66. Takahashi, R., and T. Okajima. 2015. Mapping power-law rheology of living cells using multi-frequency force modulation atomic force microscopy. Appl. Phys. Lett. 107.
67. Bufi, N., M. Saitakis, S. Dogniaux, O. Buschinger, A. Bohineust, A. Richert, M. Maurin, C. Hivroz, and A. Asnacios. 2015. Human primary immune cells exhibit distinct mechanical properties that are modified by inflammation. Biophys. J. 108: 2181–2190.
68. Tsai, M.A., R.E. Waugh, and P.C. Keng. 1998. Passive Mechanical Behavior of Human Neutrophils: Effects of Colchicine and Paclitaxel. Biophys. J. 74: 3282–3291.
69. Tsai, M.A., R.S. Frank, and R.E. Waugh. 1994. Passive mechanical behavior of human neutrophils: effect of cytochalasin B. Biophys. J. 66: 2166–2172.
70. Needham, D., and R.M.M. Hochmuth. 1992. A sensitive measure of surface stress in the resting neutrophil. Biophys. J. 61: 1664–1670.
71. Evans, E., and A. Yeung. 1989. Apparent viscosity and cortical tension of blood granulocytes determined by micropipet aspiration. Biophys. J. 56: 151–160.
72. Garcia, P.D., C.R. Guerrero, and R. Garcia. 2017. Time-resolved nanomechanics of a single cell under the depolymerization of the cytoskeleton. Nanoscale. 9: 12051–12059.
73. Sung, K.P., L.A. Sung, M. Crimmins, S.J. Burakoff, and S.H.U. Chien. 1986. Dynamic changes in viscoelastic properties in cytotoxic T-lymphocyte- mediated killing. J. Cell Sci. 91: 179–189.
74. Lipowsky, H.H., D. Riedel, and G.S. Shi. 1991. In vivo mechanical properties of leukocytes during adhesion to venular endothelium. Biorheology. 28: 53–64.
75. Wang, N., I.M. Tolić-Nørrelykke, J. Chen, S.M. Mijailovich, J.P. Butler, J.J. Fredberg, and D. Stamenović. 2002. Cell prestress. I. Stiffness and prestress are closely associated in adherent contractile cells. Am. J. Physiol. Physiol. 282: C606–C616.
76. MacKay, J.L., A.J. Keung, and S. Kumar. 2012. A genetic strategy for the dynamic and graded control of cell mechanics, motility, and matrix remodeling. Biophys. J. 102: 434–442.
77. Wang, N., K. Naruse, D. Stamenovic, J.J. Fredberg, S.M. Mijailovich, I.M. Tolic-Norrelykke, T. Polte, R. Mannix, D.E. Ingber, S.M. Mijailovic, G. Maksym, T. Polte, D.E. Ingber, D. Stamenović, S.M. Mijailovich, I.M. Tolić-Nørrelykke, and R. Mannix. 2001. Mechanical behavior in living cells consistent with the tensegrity model. Proc. Natl. Acad. Sci. 98: 7765–70.
78. Stamenović, D., Z. Liang, J. Chen, and N. Wang. 2015. Effect of the cytoskeletal prestress on the mechanical impedance of cultured airway smooth muscle cells. J. Appl. Physiol. 92: 1443–1450.
79. Shroff, S.G., D.R. Saner, and R. Lal. 2017. Dynamic micromechanical properties of cultured rat atrial myocytes measured by atomic force microscopy. Am. J. Physiol. Physiol. 269: C286–C292.
80. Étienne, J., J. Fouchard, D. Mitrossilis, N. Bufi, P. Durand-Smet, and A. Asnacios. 2015. Cells as liquid motors: Mechanosensitivity emerges from collective dynamics of actomyosin cortex. Proc. Natl. Acad. Sci. 112: 2740–2745.
81. Mitrossilis, D., J. Fouchard, A. Guiroy, N. Desprat, N. Rodriguez, B. Fabry, and A. Asnacios. 2009. Single-cell response to stiffness exhibits muscle-like behavior. Proc. Natl. Acad. Sci. U. S. A. 106: 18243–8.
82. Simon, S.I., and G.W. Schmid-Schönbein. 1988. Biophysical aspects of microsphere engulfment by human neutrophils. Biophys. J. 53: 163–173.
83. Lomakin, A.J., K.C. Lee, S.J. Han, D.A. Bui, M. Davidson, A. Mogilner, and G. Danuser. 2015. Competition for actin between two distinct F-actin networks defines a bistable switch for cell polarization. Nat. Cell Biol. 17: 1435–1445.
84. Fritzsche, M., R.A. Fernandes, V.T. Chang, H. Colin-York, M.P. Clausen, J.H. Felce, S. Galiani, C. Erlenkämper, A.M. Santos, J.M. Heddleston, I. Pedroza-Pacheco, D. Waithe, J.B. de la Serna, B.C. Lagerholm, T.L. Liu, T.-L.L. Chew, E. Betzig, S.J. Davis, C. Eggeling, B. Christoffer Lagerholm, T.L. Liu, T.-L.L. Chew, E. Betzig, S.J. Davis, and C. Eggeling. 2017. Cytoskeletal actin dynamics shape a ramifying actin network underpinning immunological synapse formation. Sci. Adv. 3: e1603032.
85. Yeung, a, and E. Evans. 1989. Cortical shell-liquid core model for passive flow of liquid-like spherical cells into micropipets. Biophys. J. 56: 139–149.
86. Tsopoulidis, N., S. Kaw, V. Laketa, S. Kutscheidt, C. Baarlink, B. Stolp, R. Grosse, and O.T. Fackler. 2019. T cell receptor–triggered nuclear actin network formation drives CD4+ T cell effector functions. Sci. Immunol. 4.
87. Fritzsche, M., D. Li, H. Colin-York, V.T. Chang, E. Moeendarbary, J.H. Felce, E. Sezgin, G. Charras, E. Betzig, and C. Eggeling. 2017. Self-organizing actin patterns shape membrane architecture but not cell mechanics. Nat. Commun. 8: 17–19.

88. Ritter, A.T., Y. Asano, J.C. Stinchcombe, N.M.G.G. Dieckmann, B.C. Chen, C. Gawden-Bone, S. van Engelenburg, W. Legant, L. Gao, M.W. Davidson, E. Betzig, J. Lippincott-Schwartz, and G.M. Griffiths. 2015. Actin Depletion Initiates Events Leading to Granule Secretion at the Immunological Synapse. Immunity. 42: 864–876.
89. Quintana, A., C. Schwindling, A.S. Wenning, U. Becherer, J. Rettig, E.C. Schwarz, and M. Hoth. 2007. T cell activation requires mitochondrial translocation to the immunological synapse. Proc. Natl. Acad. Sci. 104: 14418–14423.
90. Wu, Z., M. Su, C. Tong, M. Wu, and J. Liu. 2018. Membrane shape-mediated wave propagation of cortical protein dynamics. Nat. Commun. 9: 1–12.
91. Freeman, S.A., A. Vega, M. Riedl, R.F. Collins, P.P. Ostrowski, E.C. Woods, C.R. Bertozzi, M.I. Tammi, D.S. Lidke, P. Johnson, S. Mayor, K. Jaqaman, and S. Grinstein. 2018. Transmembrane Pickets Connect Cyto- and Pericellular Skeletons Forming Barriers to Receptor Engagement. Cell. 172: 305-317.e10.
92. Maxson, M.E., X. Naj, T.R. O'Meara, J.D. Plumb, L.E. Cowen, and S. Grinstein. 2018. Integrin-based diffusion barrier separates membrane domains enabling the formation of microbiostatic frustrated phagosomes. Elife. 7: 1–37.
93. Siokis, A., P.A. Robert, P. Demetriou, M.L. Dustin, and M. Meyer-Hermann. 2018. F-Actin-Driven CD28-CD80 Localization in the Immune Synapse. Cell Rep. 24: 1151–1162.
94. DeMond, A.L., K.D. Mossman, T. Starr, M.L. Dustin, and J.T. Groves. 2008. T cell receptor microcluster transport through molecular mazes reveals mechanism of translocation. Biophys. J. 94: 3286–3292.
95. Mey, I., A. Janshoff, J. Rother, H. No, H. Noding, I. Mey, and A. Janshoff. 2014. Atomic force microscopy-based microrheology reveals significant differences in the viscoelastic response between malign and benign cell lines. Open Biol. 4: 140046–140046.
96. Thoumine, O., O. Cardoso, and J.J. Meister. 1999. Changes in the mechanical properties of fibroblasts during spreading: A micromanipulation study. Eur. Biophys. J. 28: 222–234.
97. Abidine, Y., A. Constantinescu, V.M. Laurent, V. Sundar Rajan, R. Michel, V. Laplaud, A. Duperray, C. Verdier, R. Michel, V.M. Laurent, V. Sundar Rajan, C. Verdier, A. Duperray, Y. Abidine, A. Constantinescu, V.M. Laurent, V. Sundar Rajan, R. Michel, V. Laplaud, A. Duperray, and C. Verdier. 2018. Mechanosensitivity of Cancer Cells in Contact with Soft Substrates Using AFM. Biophys. J. 114: 1165–1175.